International Journal of Solids and Structures 46 (2009) 2060–2074

Contents lists available at ScienceDirect

International Journal of Solids and Structures

journal homepage: www.elsevier.com/locate/ijsolstr

Topology optimization of a plate coupled with acoustic cavity

W. Akl [a], A. El-Sabbagh [a], K. Al-Mitani [b], A. Baz [b,*]

[a] Design and Production Engineering Department, Ain Shams University, Cairo, Egypt
[b] Mechanical Engineering Department, University of Maryland, 2137 Engineering Bldg., College Park, MD 20742, USA

ARTICLE INFO

Article history:
Received 3 March 2008
Received in revised form 20 May 2008
Available online 10 June 2008

This paper is dedicated to the memory of Professor Liviu Librescu who has touched and enriched our lives as a great scholar, consummate professional, and most importantly as a wonderful friend

Keywords:
Topology optimization
Fluid–structure interactions
Acoustic cavity
Finite element
Experimental validation

ABSTRACT

Optimization of the topology of a plate coupled with an acoustic cavity is presented in an attempt to minimize the fluid–structure interactions at different structural frequencies. A mathematical model is developed to simulate such fluid–structure interactions based on the theory of finite elements. The model is integrated with a topology optimization approach which utilizes the moving asymptotes method. The obtained results demonstrate the effectiveness of the proposed approach in simultaneously attenuating the structural vibration and the sound pressure inside the acoustic domain at several structural frequencies by proper redistribution of the plate material.

Experimental verification is carried out by manufacturing topology optimized plates and monitoring their vibration and sound radiation into a rigid acoustic cavity. The measured sound pressure and plate vibration are found to be in good agreement with the predictions of the mathematical model.

The presented theoretical and experimental techniques present valuable tools in the design of a wide variety of critical structures which must operate quietly when subjected to fluid loading.

1. Introduction

In recent years, extensive application of topology optimization to continuum structures has been reported, as it has been recognized that using such an approach yields to improved static and dynamic characteristics. For these reasons, topology optimization has found its ways in aeronautical, civil and mechanical engineering applications, and started to become a standard module of commercial finite element packages.

The literature on structural topology optimization is quite extensive and the research activities in this field have focused on a wide variety of applications. The optimization problem was treated as a material distribution problem to minimize/maximize certain objective functions. In other words, the structural material is redistributed to achieve the optimization goal bounded by various constraints, among which is the volume fraction of the material. The efficiency of this method was clearly demonstrated by solving the classical problem of minimizing the compliance of various structures (Bendsoe and Kikuchi, 1988; Bendsoe, 1989) and maximizing their fundamental buckling load (Bendsoe and Sigmund, 2003). Later on, structural dynamics started to become the focus of researchers working in topology optimization. Maximization of the structural dynamics properties such as the eigenfrequencies and maximizing the gap between two consecutive eigenfrequencies was tackled by Bendsoe and Diaz (1994), Krog and Olhoff (1999), Pederson (2000), Olhoff and Du (2005) and Jensen and Pedersen (2006). Minimizing the dynamical response of a structure for a given driving frequency or frequency range was studied by Jog (2002).

However, fewer studies have considered the application of topology optimization to fluid–structure interaction problems. For example, Yoon et al. (2007) used a mixed finite element model to represent a fluid–structure coupled domain, where the

* Corresponding author. Tel.: +1 301 405 5216; fax: +1 301 405 8331.
E-mail address: baz@eng.umd.edu (A. Baz).

0020-7683/$ - see front matter © 2008 Elsevier Ltd. All rights reserved.
doi:10.1016/j.ijsolstr.2008.05.034

Nomenclature

List of symbols

A	fluid–structure boundary area
A^e	surface area for structure finite element
c	sonic speed in the acoustic medium
f_{st}	externally applied mechanical force on the structure
h^e	plate finite element thickness
$h_{max,min}$	maximum and minimum permissible plate thickness
J	performance index
K.E.	kinetic energy
$[\mathbf{K_A}]$, $[\mathbf{K_s}]$	stiffness matrix of the acoustic cavity and structure
$[\mathbf{M_A}]$, $[\mathbf{M_s}]$	mass matrix of the acoustic cavity and structure
N^e	number of elements in the plate structure
N_w, N_ϕ	shape functions for the plate transverse displacement and the velocity potential
P.E.	potential energy
p, $\{\mathbf{p}\}$	acoustic pressure and nodal pressure vector in the acoustic domain
u_A	particle displacement in the acoustic medium
V	volume of fluid
v_f	volume fraction
w	transverse displacement of the plate
$\mathbf{W_P}$	work done on the acoustic cavity by the plate elements
$\{\boldsymbol{\delta}\}$	degrees of freedom for the structure element
θ_x, θ_y	rotation of the node about the x and y axes
ρ_A, ρ	density of the acoustic medium and structure
ϕ	velocity potential in the acoustic domain
$[\Omega_P]$	fluid–structure coupling matrix
ω	angular velocity

structure was placed inside an acoustic medium. Using this approach, the authors were able to formulate the problem without explicit boundary interface representation. The objective of the optimization scheme was to minimize the sound pressure inside the acoustic medium, when exciting the structure by fixed excitation frequency. Du and Olhoff (2007) have attempted to minimize the sound power radiated from a structure surface placed inside an acoustic cavity. However, because air was the acoustic medium, a feedback coupling between the acoustic medium and the structure was neglected. In addition, weak coupling was assumed and the acoustic pressure was ignored in the structural equations. Also, in their study the excitation frequency was maintained fixed at certain value regardless of the effect that the material redistribution has on the stiffness of the structure domain, and on the modal frequencies.

Hence, topology optimization of fluid–structure interaction problems, where true coupling is considered and the external excitation being locked to the modal frequencies has yet to considered. It is therefore the objective of the current paper to model a fluid–structure interaction problem, where a vibrating flexible plate is coupled to a closed acoustic cavity. A topology optimization approach using the method of moving asymptotes (MMA) (Svanberg, 1999; Bruyneel et al., 2002) will be developed to minimize the coupling between the flexible plate and the acoustic domain. Doing so, the energy transfer between the two domains will be minimized. All of this is considered at modal frequencies, since it is clear, that during the optimization phase the material distribution varies from iteration to the next, affecting consequently the natural frequencies of the fluid-loaded structure. In this case, the true attenuation of the structural vibration and the associated sound radiation can be attributed only to the effect of the topology optimization and not to the shift of the natural frequencies.

This paper is organized in six sections. In Section 1, a brief introduction has been presented. The mathematical model describing the fluid–structure interaction between the plate and the acoustic cavity is presented in Section 2. The formulation of the topology optimization problem is developed in Section 3. The theoretical and experimental performance characteristics of the topology optimized plate/cavity system are presented in Sections 4 and 5 respectively. A brief summary of the conclusions is given in Section 6.

2. Modeling of plate–cavity interaction

2.1. Overview

Consider the plate–cavity system shown schematically in Fig. 1. In this system, a rectangular flexible plate is coupled with an acoustic cavity that has five rigid walls. The plate is subjected to external excitation and a finite element model will be developed to predict the interaction between the plate vibration and the associated sound radiation into the acoustic cavity.

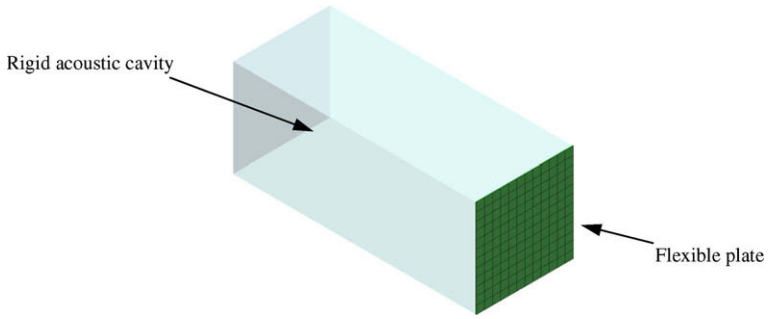

Fig. 1. Coupled plate–cavity system.

The finite element model consists of two different types of elements. The first one is 4-node quad elements with 3 degrees of freedom per node (w, θ_x, θ_y) representing the transverse displacement of the node and rotations about the x-axis and the y-axis, respectively. The second type of elements is a cubic 8-node element for the acoustic domain with the acoustic pressure (p) as the sole degree of freedom per node. The element shapes are as presented in Figs. 2 and 3.

2.2. Individual models of the plate and cavity

2.2.1. The cavity

Considering a fluid volume "V", then the following identities can be defined:

$$\text{Potential energy } (\mathbf{P}.\mathbf{E}.) = \frac{1}{2}\rho_A c^2 \int_V (\text{div} u_A)^2 dV, \tag{1}$$

$$\text{Kinetic energy } (\mathbf{K}.\mathbf{E}.) = \frac{1}{2}\rho_A \int_V \dot{u}_A^2 dV. \tag{2}$$

The work done on the acoustic cavity by the plate element is given by

$$(\mathbf{W_P}) = \int_{\text{BoundaryArea}} pw dA. \tag{3}$$

For the sake of simplifying the calculations, the velocity potential φ (a scalar quantity) is used instead of the acoustic pressure p using the following identities:

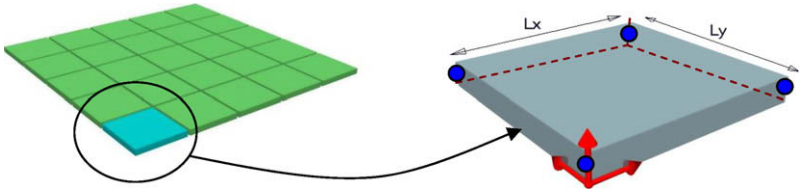

Fig. 2. Plate 4-node quad element.

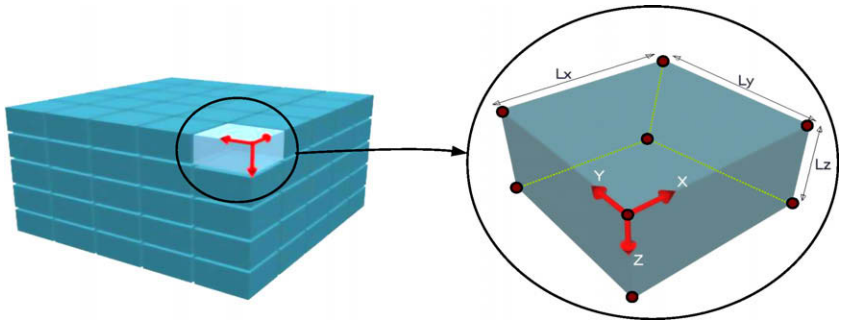

Fig. 3. Acoustic 8-node brick element.

$$\bullet p = -\rho_A \frac{\partial \varphi}{\partial t}, \tag{4}$$

$$\bullet \dot{u}_A = -\nabla \varphi = -\left[\frac{\partial \varphi}{\partial x}\,\vec{i} + + \frac{\partial \varphi}{\partial y}\,\vec{j} + \frac{\partial \varphi}{\partial z}\,\vec{k}\right], \tag{5}$$

$$\bullet \dot{u}_A^2 = (-\nabla \varphi)^2 = \left[\left(\frac{\partial \varphi}{\partial x}\right)^2 + \left(\frac{\partial \varphi}{\partial y}\right)^2 + \left(\frac{\partial \varphi}{\partial z}\right)^2\right], \tag{6}$$

$$\bullet \mathrm{div} u_A = -\frac{1}{c^2}\frac{\partial \varphi}{\partial t}. \tag{7}$$

$$\text{Hence, } \mathbf{P.E.} = \frac{1}{2}\frac{\rho_A}{c^2}\int_V \dot{\varphi}^2 \mathrm{d}V, \tag{8}$$

$$\mathbf{K.E.} = \frac{1}{2}\rho_A \int_V (\nabla \varphi)^2 \mathrm{d}V, \tag{9}$$

$$\text{and } \mathbf{W_P} = -\rho_A \int_{\text{BoundaryArea}} \varphi^{\bullet} w \mathrm{d}A. \tag{10}$$

Hamilton's principle, as given by Eq. (11), is used to extract the differential equation of motion of the acoustic fluid, as influenced by the coupling with the plate:

$$\int_{t_1}^{t_2} \delta(\mathbf{K.E.} - \mathbf{P.E.} + \mathbf{W_P})\mathrm{d}t = 0. \tag{11}$$

Let $\varphi = N_\phi \boldsymbol{\varphi}$ where N_φ denotes an appropriate shape function and $\boldsymbol{\varphi}$ represents the nodal velocity potential vector of the element. Similarly, let $w = N_w\{\boldsymbol{\delta}\}$ where N_w is an appropriate shape function and $\{\boldsymbol{\delta}\}$ denotes the nodal deflection vector of the plate. Then

The variation of the potential energy (δ **P.E.**)

$$\int_{t_1}^{t_2} \delta(\mathbf{P.E.})\mathrm{d}t = \frac{\rho_A}{c^2}\int_{t_1}^{t_2}\int_V \{\boldsymbol{\delta}\dot{\boldsymbol{\varphi}}\}^T[(N_\varphi)^T(N_\varphi)]\{\dot{\boldsymbol{\varphi}}\}\mathrm{d}V\mathrm{d}t. \tag{12}$$

Integrating Eq. (12) by parts to eliminate $\{\delta\dot{\boldsymbol{\varphi}}\}$ yields

$$\int_{t_1}^{t_2} \delta(\mathbf{P.E.})\mathrm{d}t = -\frac{\rho_A}{c^2}\int_{t_1}^{t_2}\int_V \{\boldsymbol{\delta}\boldsymbol{\varphi}\}^T[(N_\varphi)^T(N_\varphi)]\{\ddot{\boldsymbol{\varphi}}\}\mathrm{d}V\mathrm{d}t. \tag{13}$$

Similarly, the variation of the kinetic energy (δ **K.E.**):

$$\int_{t_1}^{t_2} \delta(\mathbf{K.E.})\mathrm{d}t = \rho_A \int_{t_1}^{t_2}\int_V \{\boldsymbol{\delta}\boldsymbol{\varphi}\}^T[(\nabla N_\varphi)^T(\nabla N_\varphi)]\{\boldsymbol{\varphi}\}\mathrm{d}V\mathrm{d}t, \tag{14}$$

and the variation of the work done by the plate (δ $\mathbf{W_P}$) can be determined as follows:

$$\text{As } \mathbf{W_P} = -\rho_A \int_A \{\dot{\boldsymbol{\varphi}}\}^T(N_\varphi)^T(N_w)\{\boldsymbol{\delta}\}\mathrm{d}A, \tag{15}$$

$$\text{then } \int_{t_1}^{t_2} \delta(\mathbf{W_P})\mathrm{d}t = -\rho_A \int_{t_1}^{t_2}\int_A \{\boldsymbol{\delta}\dot{\boldsymbol{\varphi}}\}^T[(N_\varphi)^T(N_w)]\{\boldsymbol{\delta}\}\mathrm{d}A\mathrm{d}t, \tag{16}$$

$$\text{or } \int_{t_1}^{t_2} \delta(\mathbf{W_P})\mathrm{d}t = -\rho_A \int_{t_1}^{t_2}\int_A \{\boldsymbol{\delta}\boldsymbol{\varphi}\}^T[(N_\varphi)^T(N_w)]\{\dot{\boldsymbol{\delta}}\}\mathrm{d}A\mathrm{d}t. \tag{17}$$

Finally, summing up the terms of $\{\delta\boldsymbol{\varphi}\}$ inside the time integral and equating them to zero results in the required equation of motion of the acoustic element:

$$\frac{\rho_A}{c^2}\int_V (N_\varphi)^T(N_\varphi)\mathrm{d}V\{\ddot{\boldsymbol{\varphi}}\} + \rho_A \int_V (\nabla N_\varphi)^T(\nabla N_\varphi)\mathrm{d}V\{\boldsymbol{\varphi}\} = \rho_A \int_A (N_\varphi)^T(N_w)\mathrm{d}A\{\dot{\boldsymbol{\delta}}\}. \tag{18}$$

Differentiating with respect to time and utilizing the following identities:

$$\begin{array}{l} \dot{\varphi} = -\frac{p}{\rho_A}, \quad \ddot{\varphi} = -\frac{\dot{p}}{\rho_A}, \quad \text{and} \quad \dddot{\varphi} = -\frac{\ddot{p}}{\rho_A} \\ \text{gives} \quad \frac{1}{c^2}\int_V (N_\varphi)^T(N_\varphi)\mathrm{d}V\{\ddot{\mathbf{p}}\} + \int_V (\nabla N_\varphi)^T(\nabla N_\varphi)\mathrm{d}V\{\mathbf{p}\} = -\rho_A \int_A (N_\varphi)^T(N_w)\mathrm{d}A\{\ddot{\boldsymbol{\delta}}\} \end{array}, \tag{19}$$

where $\{\mathbf{p}\}$ is the nodal pressure vector, which could also be written as

$$[\mathbf{M_A}]\{\ddot{\mathbf{p}}\} + [\mathbf{K_A}]\{\mathbf{p}\} = -[\boldsymbol{\Omega}]^T\{\ddot{\boldsymbol{\delta}}\}, \tag{20}$$

where

- $\{\boldsymbol{\delta}\}$ = the degrees of freedom of the structure element,
- $[\mathbf{M_A}] = \frac{1}{c^2}\int_V (N_\varphi)^{\mathrm{T}}(N_\varphi)\mathrm{d}V$ = the mass matrix of the acoustic medium,
- $[\mathbf{K_A}] = \int_V (\nabla N_\varphi)^{\mathrm{T}}(\nabla N_\varphi)\mathrm{d}V$ = the stiffness matrix of the acoustic medium,
- $[\Omega]^{\mathrm{T}} = \rho_{\mathrm{A}}\int_A [(N_\varphi)^{\mathrm{T}}(N_{\mathrm{w}})]\mathrm{d}A$ = the fluid–structure coupling matrix.

2.2.2. The plate

The plate finite element model is based on the first order shear deformation theory, which is efficiently used for relatively thick as well as thin plates. In this model, it is assumed that planes normal to the mid-surface of the plate in the un-deformed state remain plane but not necessarily normal to the mid-surface in the deformed state. Hence the rotation degrees of freedom (θ_x, θ_y) are considered as independent degrees of freedom and not derivatives of the mid-surface out of plane displacements.

Then, the equation of motion of the plate is given as

$$[\mathbf{M_s}]\{\ddot{\boldsymbol{\delta}}\} + [\mathbf{K_s}]\{\boldsymbol{\delta}\} = F_{\mathrm{S}}, \tag{21}$$

where F_{S} represent the forces exerted by the acoustic fluid on the plate elements.

The forcing function "F_{S}" can be calculated from the work done by the acoustic field on the structure as follows:

$$\mathbf{W_P} = \int_{\mathrm{BoundaryArea}} wp\mathrm{d}A \tag{22}$$

$$\mathbf{W_P} = \int_A \{\boldsymbol{\delta}\}^{\mathrm{T}}(N_{\mathrm{w}})^{\mathrm{T}}(N_\varphi)\{\mathbf{p}\}\mathrm{d}A \tag{23}$$

$$\text{Hence, } \int_{t_1}^{t_2} \delta(\mathbf{W_P})\mathrm{d}t = \int_{t_1}^{t_2}\int_A [\{\delta\boldsymbol{\delta}\}^{\mathrm{T}}(N_{\mathrm{w}})^{\mathrm{T}}(N_\varphi)\{\mathbf{p}\}\mathrm{d}A]\mathrm{d}t. \tag{24}$$

Since the work = force × displacement, then the forcing term on the plate can be calculated as

$$F_{\mathrm{S}} = \frac{[\Omega]\mathbf{p}}{\rho_{\mathrm{A}}} \quad \text{with} \quad [\Omega] = \rho_{\mathrm{A}}\int_A (N_{\mathrm{w}})^{\mathrm{T}}(N_\varphi)\mathrm{d}A.$$

Thus, the complete differential equation of the plate is given as

$$[\mathbf{M_s}]\{\ddot{\boldsymbol{\delta}}\} + [\mathbf{K_s}]\{\boldsymbol{\delta}\} = \frac{[\Omega]\{\mathbf{p}\}}{\rho_{\mathrm{A}}}. \tag{25}$$

2.3. Coupling the acoustic cavity with the plate structure

The equation of motion of the coupled system is given in the following matrix form

$$\begin{pmatrix} \mathbf{M_s} & 0 \\ [\Omega]^{\mathrm{T}} & \mathbf{M_A} \end{pmatrix}\begin{Bmatrix} \ddot{\boldsymbol{\delta}} \\ \ddot{\mathbf{p}} \end{Bmatrix} + \begin{pmatrix} \mathbf{K_s} & -[\Omega]/\rho_{\mathrm{A}} \\ 0 & \mathbf{K_A} \end{pmatrix}\begin{Bmatrix} \boldsymbol{\delta} \\ \mathbf{p} \end{Bmatrix} = \begin{Bmatrix} f_{\mathrm{s}} \\ 0 \end{Bmatrix}, \tag{26}$$

where, "f_{s} " is the externally applied force.

From (26) for harmonic excitation at angular frequency ω

$$(\mathbf{K_s} - \mathbf{M_s}\boldsymbol{\omega^2})\boldsymbol{\delta} - \frac{[\boldsymbol{\Omega}]}{\rho_{\mathrm{A}}}\mathbf{p} = \mathbf{f_s} \tag{27}$$

$$\text{or, } \mathbf{p} = (\mathbf{K_A} - \mathbf{M_A}\boldsymbol{\omega^2})^{-1}\omega^2[\boldsymbol{\Omega}]^{\mathbf{T}}\boldsymbol{\delta}. \tag{28}$$

Substituting for $\mathbf{p}$ from (28) into (27) results in

$$\left[(\mathbf{K_s} - \mathbf{M_s}\boldsymbol{\omega^2}) - \frac{[\boldsymbol{\Omega}]}{\rho_{\mathrm{A}}}(\mathbf{K_A} - \mathbf{M_A}\boldsymbol{\omega^2})^{-1}\omega^2[\boldsymbol{\Omega}]^{\mathbf{T}}\right]\boldsymbol{\delta} = \mathbf{f_s}. \tag{29}$$

It is important here to note that a boundary layer is inserted at the interface between the plate and the cavity as shown in Fig. 4. This boundary layer accommodates the changes between the plate nodal DOF (w, θ_x, θ_y) and the cavity nodal DOF (p). In this layer, the out of plane displacement of the plate causes the adjacent fluid to move with the same velocity in a direction normal to the plate surface, thus resulting in a pressure variation inside that layer which is then transmitted to neighboring fluid elements. In return, the plate is loaded with the fluid mass adjacent to resulting in variation of the stiffness and mass of the fluid loaded plate. Therefore the coupling matrix "Ω", described in Eqs. (20) and (25), is developed to account for this mutual interaction.

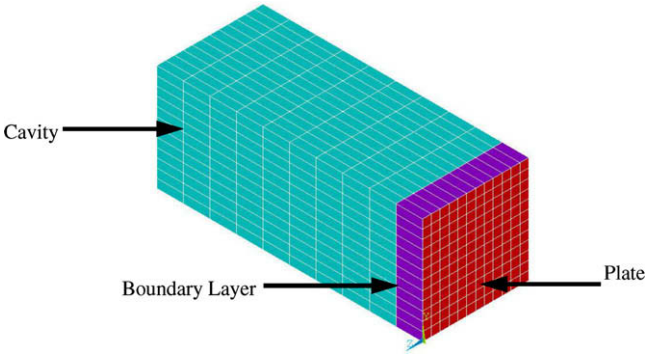

Fig. 4. Interaction between the plate and the acoustic cavity.

3. Formulation of the optimization of the fluid–structure interaction problem

3.1. Problem formulation

The topology optimization problem can be formulated as follows:

$$\min_{\rho} J = (\boldsymbol{\delta}^{\mathbf{T}} C_{\mathrm{w}}^{\mathrm{T}} \mathbf{p}) \text{ defined at the boundary area}$$

$$\left\langle \text{such that } \begin{pmatrix} \mathbf{M_{st}} & \mathbf{0} \\ [\boldsymbol{\Omega}]^{\mathbf{T}} & \mathbf{M_A} \end{pmatrix} \begin{Bmatrix} \ddot{\boldsymbol{\delta}} \\ \ddot{\mathbf{p}} \end{Bmatrix} + \begin{pmatrix} \mathbf{K_{st}} & -[\boldsymbol{\Omega}]/\rho_{\mathrm{A}} \\ \mathbf{0} & \mathbf{K_A} \end{pmatrix} \begin{Bmatrix} \boldsymbol{\delta} \\ \mathbf{p} \end{Bmatrix} = \begin{Bmatrix} \mathbf{f_s} \\ \mathbf{0} \end{Bmatrix}, \right\rangle.$$

$$\sum_{e=1}^{N_e} h^e A^e \leqslant v_{\mathrm{f}} \times h_{\max} \times \sum_{e=1}^{N_e} A^e$$

$$0 < h_{\min} < h^e < h_{\max}$$

Note that $C_{\mathrm{w}}\boldsymbol{\delta} = \mathbf{w}$ where C_{w} is a matrix that extracts the transverse deflection $\mathbf{w}$ from the nodal deflection vector $\boldsymbol{\delta}$. Also, the objective function can be explained literally as to minimize the coupling between the structure and the fluid domains. By doing this, minimum work or energy is transmitted between the structure and the fluid domains, resulting in minimization of the sound intensity and sound pressure levels, due to structure resonances inside the acoustic cavity. It is worth mentioning, that due to the formulated objective function, the cavity modes will not be affected as a result of the topology optimization of the flexible plate.

3.2. Sensitivity analysis

The sensitivity of the objective function "J" which defines the fluid–structure coupling, with respect to the optimization variable (plate element density "ρ") is given as follows:

$$\frac{\mathrm{d}J}{\mathrm{d}\rho} = \boldsymbol{\delta}^{\mathrm{T}} C_{\mathrm{w}}^{\mathrm{T}} \frac{\mathrm{d}\mathbf{p}}{\mathrm{d}\rho} + \mathbf{p}^{\mathbf{T}} C_{\mathrm{w}} \frac{\mathrm{d}\boldsymbol{\delta}}{\mathrm{d}\rho}. \tag{30}$$

To calculate $\frac{\mathrm{d}\delta}{\mathrm{d}\rho}$ we differentiate Eq. (29) w.r.t. ρ. This yields

$$\frac{\mathrm{d}\left[\left\{(\mathbf{K_s} - \mathbf{M_s}\omega^{\mathbf{2}}) - \frac{[\boldsymbol{\Omega}]}{\rho_{\mathrm{A}}}(\mathbf{K_A} - \mathbf{M_A}\omega^{\mathbf{2}})^{-\mathbf{1}}\omega^2[\boldsymbol{\Omega}]^{\mathbf{T}}\right\}\boldsymbol{\delta}\right]}{\mathrm{d}\rho} = \frac{\mathrm{d}f_{\mathrm{s}}}{\mathrm{d}\rho} = 0.$$

Define $\mathbf{K_{s\_D}} = (\mathbf{K_s} - \mathbf{M_s}\omega^{\mathbf{2}})$, $\mathbf{K_{fl\_D}} = (\mathbf{K_A} - \mathbf{M_A}\omega^{\mathbf{2}})$, $\mathbf{A} = \frac{[\boldsymbol{\Omega}]}{\rho_{\mathrm{A}}}(\mathbf{K_A} - \mathbf{M_A}\omega^{\mathbf{2}})^{-\mathbf{1}}\omega^2[\boldsymbol{\Omega}]^{\mathbf{T}}$

$$\frac{\mathrm{d}\mathbf{K_{s\_D}}}{\mathrm{d}\rho}\boldsymbol{\delta} + [\mathbf{K_{s\_D}} - \mathbf{A}]\frac{\mathrm{d}\boldsymbol{\delta}}{\mathrm{d}\rho} = 0, \quad \mathbf{B} = [\mathbf{K_{s\_D}} - \mathbf{A}], C = \frac{\mathrm{d}\mathbf{K_{s\_D}}}{\mathrm{d}\rho}. \tag{31}$$

Hence, $\frac{\mathrm{d}\delta}{\mathrm{d}\rho} = -\mathbf{B}^{-\mathbf{1}}\mathbf{C}\boldsymbol{\delta}$.

To calculate $\frac{\mathrm{d}\mathbf{p}}{\mathrm{d}\rho}$ we differentiate Eq. (28) with respect to ρ gives

$$\omega^2[\boldsymbol{\Omega}]^{\mathbf{T}}\frac{\mathrm{d}\boldsymbol{\delta}}{\mathrm{d}\rho} = (\mathbf{K_A} - \mathbf{M_A}\omega^{\mathbf{2}})\frac{\mathrm{d}\mathbf{p}}{\mathrm{d}\rho}.$$

Define $\mathbf{D} = \omega^2[\boldsymbol{\Omega}]^{\mathbf{T}}$, then $\frac{\mathrm{d}\mathbf{p}}{\mathrm{d}\rho} = \mathbf{K}_{\mathbf{fl\_D}}^{-\mathbf{1}}\mathbf{D}\frac{\mathrm{d}\delta}{\mathrm{d}\rho}$.

From Eq. (30)

$$\frac{dJ}{d\rho} = \boldsymbol{\delta}^{T} C_{w}^{T} \mathbf{K}_{\mathbf{fl\_D}}^{-\mathbf{1}} \mathbf{D} \frac{T\boldsymbol{\delta}}{T\rho} + \mathbf{p}^{T} C_{w} \frac{d\boldsymbol{\delta}}{d\rho}. \tag{32}$$

Substituting $\frac{T\delta}{T\rho}$ from Eq. (31) into (32), results in

$$\frac{TJ}{T\rho} = -(\boldsymbol{\delta}^{\mathbf{T}} C_{w}^{T} \mathbf{K}_{\mathbf{fl\_D}}^{-\mathbf{1}} \mathbf{D} \mathbf{B}^{-\mathbf{1}} \mathbf{C} \boldsymbol{\delta} + \mathbf{p}^{\mathbf{T}} C_{w} \mathbf{B}^{-\mathbf{1}} \mathbf{C} \boldsymbol{\delta}).$$

During the topology optimization calculation, the effect of the density is substituted for by the effect of the thickness of the plate elements.

4. Numerical results

4.1. Model parameters

A finite element model for a closed acoustic cavity coupled with a flexible aluminum plate was developed. The characteristics of the coupled fluid–structure domains are as given in Table 1 and as shown in Fig. 1.

In the following analysis, the excitation force is locked to the structural modal frequency under consideration so that the optimization algorithm will redistribute the material of the aluminum plate in such a way to minimize the coupling at that specific modal frequency. The excitation force applied on the aluminum plate is selected to be symmetric, and the first two odd modes are studied.

The initial plate thickness under consideration is 1/16 in. It is the objective of this study to use 50% of the material of the plate and minimize the fluid–structure coupling. Therefore, the initial guess starts with a plate with uniform thickness of 1/32 in. and while the optimization algorithm evolves, the thickness should vary between 1/16 in. and 1/64 in., which represents the minimum permissible plate thickness.

The aluminum plate is excited mechanically with external forces at frequencies locked at the modal frequencies of the coupled plate–cavity system. In specific, the first and fifth modes were considered since they represent the first two odd modes, which are known of their high acoustic coupling. At each optimization iteration, the structural modal frequencies are expected to change due to the effect of the material redistribution of the aluminum plate. Therefore, at each iteration, the structural modal frequencies of the first two odd modes for the coupled system are calculated and the excitation frequency is locked on.

4.2. Excitation frequency and topology optimization targeting the first odd mode

The shape of material distribution and relative plate displacement field progresses as shown in Fig. 5. While the actual objective function was to minimize the fluid–structure acoustic coupling, it was more realistic to monitor the effect of the optimization process on the sound intensity measured inside the acoustic cavity at the frequency of the first odd structural mode. Fig. 6 illustrates the solution convergence for the first mode optimization and its effect on the attenuation of the sound intensity.

The frequency response for the plate displacement and the sound pressure were also monitored. The plate displacement was monitored at the midpoint of the plate and the sound pressure was also calculated at a point 3" away from the midpoint of the plate inside the acoustic cavity. The frequency responses for the plain and optimized cases are as shown in Figs. 7 and 8.

4.3. Excitation frequency and topology optimization targeting the second odd mode

The shape of material distribution and relative plate displacement field progresses as shown in Fig. 9.

Again, the convergence for the sound intensity for the second odd structural mode is illustrated in Fig. 10.

The frequency response for the plate displacement and the sound pressure were again monitored at the same locations as in the first case and are plotted in Figs. 11 and 12.

Table 1
Coupled structure–fluid coupled domains parameters

Cavity dimensions	$12'' \times 12'' \times 30''$
Fluid domain	Air at 25 °C and 1 atm
Flexible plate dimensions	$12'' \times 12''$
Flexible plate thickness (h_{max})	1/16″
Flexible plate material	Aluminum
Volume fraction, v_f	0.5
h_{min}	$0.25 \times h_{max}$

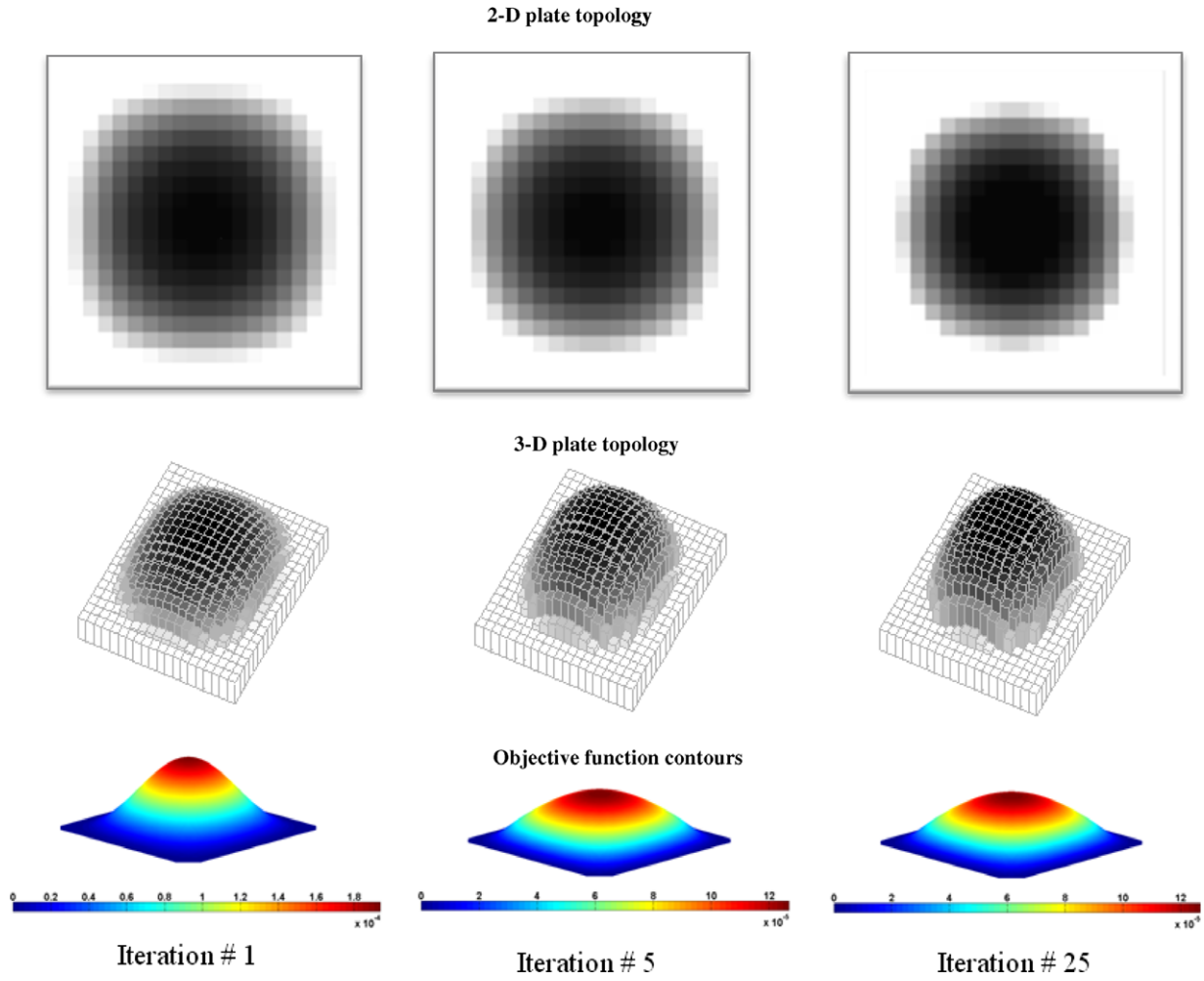

Fig. 5. Material distribution for first mode optimization.

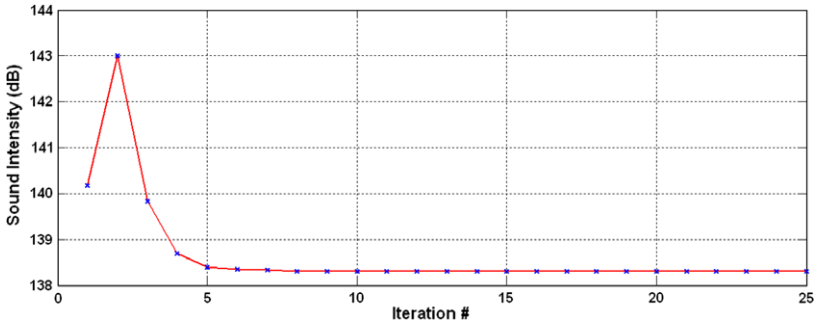

Fig. 6. Convergence of the sound intensity for first structural odd mode optimization.

It can be seen from the aforementioned figures that by exciting the aluminum plate at the first structural mode frequency, the plate displacement is considerably reduced as well as the sound pressure inside the acoustic cavity. The sound pressure attenuation at the first mode has measured above 3.5 dB. Considerable attenuation was also monitored at other structural modes. When targeting the second structural odd mode on the other hand, the sound pressure attenuation measured at that mode has recorded a value above 12 dB, although the optimization didn't significantly affect the attenuation at other structural modes.

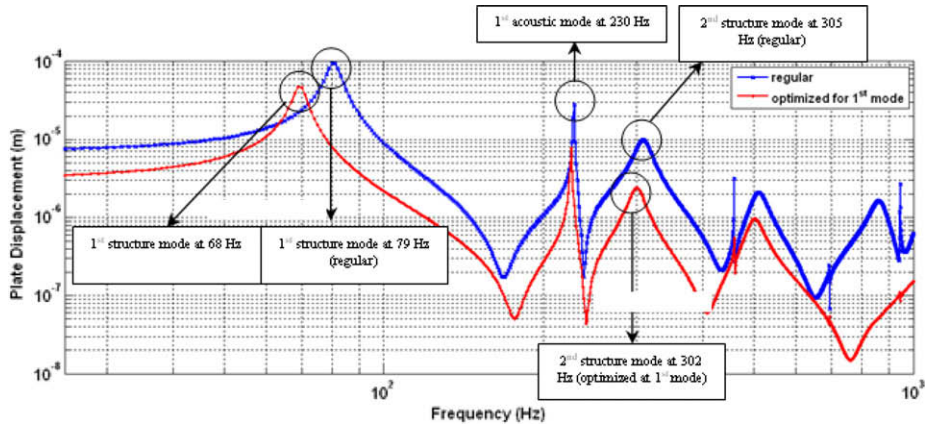

Fig. 7. Displacements of plain plate and topology optimized plate targeting first odd mode.

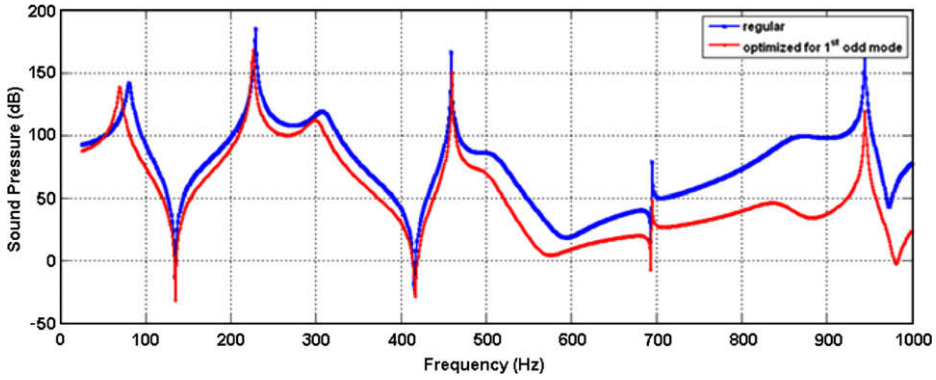

Fig. 8. Sound pressure of plain plate and topology optimized plate targeting first odd mode.

5. Experimental verification

To verify the obtained results experimentally, a set of three different Aluminum plate configurations were prepared. The first plate has surface dimensions of 12 in. × 12 in. and uniform thickness of 1/32 in. The second and third plates were manufactured from 1/64 in. Aluminum sheets to approximate the topology optimization results when targeting the first and second structural odd modes respectively, while maintaining the volume equal to the first plain case as shown in Figs. 13 and 14.

In Figs. 13 and 14, the plain uncovered metal has a thickness of 1/64 in., the while-covered parts have a thickness of 1/32 in., the red-covered parts have a thickness of 3/64 in. and finally the black-covered plate parts have a thickness of 1/16 in. Note that the plain plate weighs 254 g, topology optimized plate targeting the first mode is 252 g, and topology optimized plate targeting the fifth mode 256 g.

A 12″ × 12″ × 30″ closed acoustic cavity was prepared. The cavity has only one surface coupled to the flexible aluminum plate as shown in Fig. 15. Each of the three different plates was mounted and the plate acceleration as well as the sound pressure level inside the cavity was measured. The plate was mechanically excited with a speaker that is mounted in a position to cause the excitation to be symmetric.

The speaker was excited with a function generator that sweeps a frequency range between 40 Hz and 1 kHz with a resolution of 0.5 Hz. The acceleration was measured at the midpoint of the plate and the sound pressure was measured at a point corresponding to the midpoint of the plate, only 3 in. away.

Frequency response for the plate acceleration as well as the sound pressure inside the acoustic cavity are shown in Figs. 16 and 17 for the first case, where the optimization is tailored to the first structural odd mode.

The displayed results emphasize the effectiveness of the topology optimization in attenuating both the structural vibration of the plate and the sound pressure level inside the acoustic cavity. Furthermore, the obtained results agree closely with the theoretical predictions displayed in Figs. 7 and 8.

Figs. 18 and 19 show the corresponding results when the topology optimization is tailored to the second odd mode.

The obtained results demonstrate also the effectiveness of the topology optimization in attenuating both the structural vibration of the plate and the sound pressure level inside the acoustic cavity. Furthermore, the obtained results agree closely with the theoretical predictions displayed in Figs. 11 and 12.

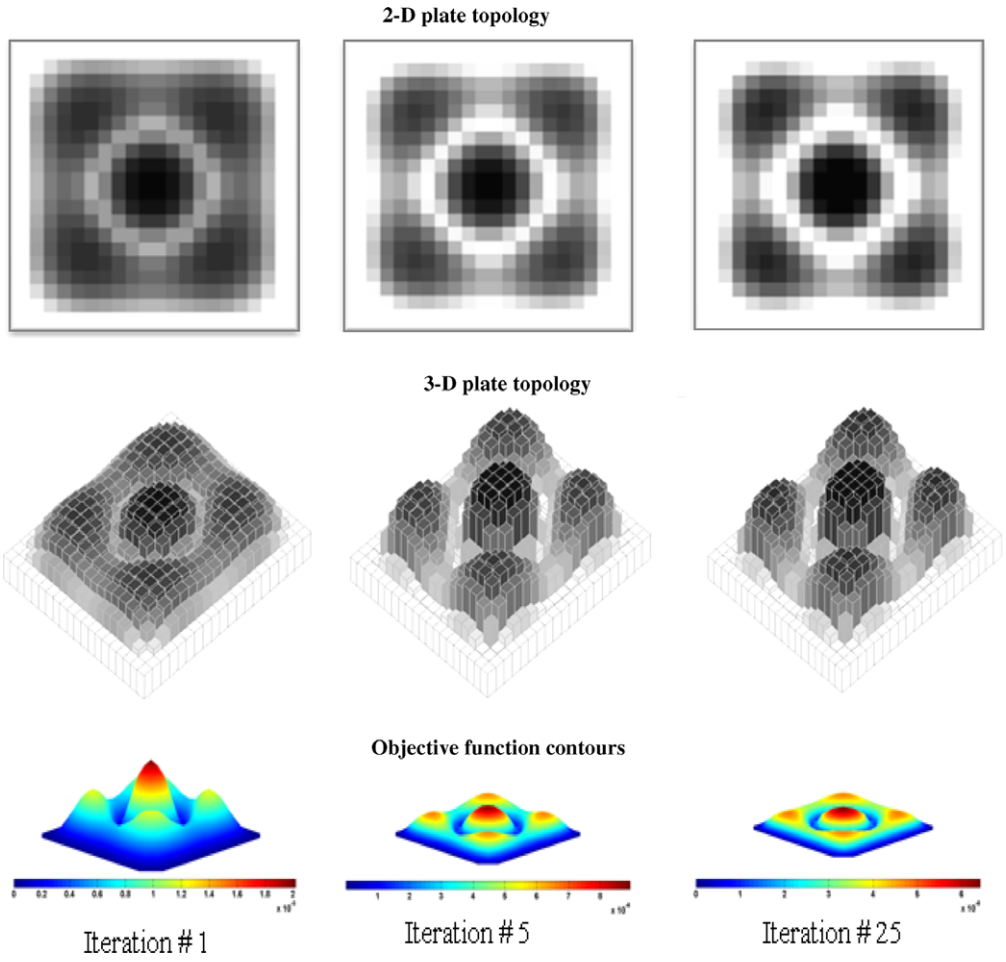

Fig. 9. Material distribution for second structural odd mode optimization.

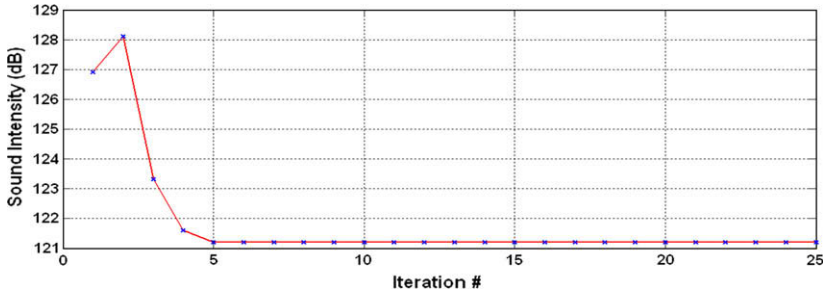

Fig. 10. Convergence of sound intensity for second structural odd mode Optimization.

In addition to frequency response measurement for the plate vibration acceleration and sound pressure inside the acoustic cavity, the plate displacement field was measured using a laser vibrometer. The setup is shown in Fig. 20.

The three plate sets were excited at the first structural odd mode using a function generator and the excitation speaker. The laser vibrometer is used to measure the displacement field of the different plates, while locked at the same excitation frequency as shown in Figs. 21 and 22.

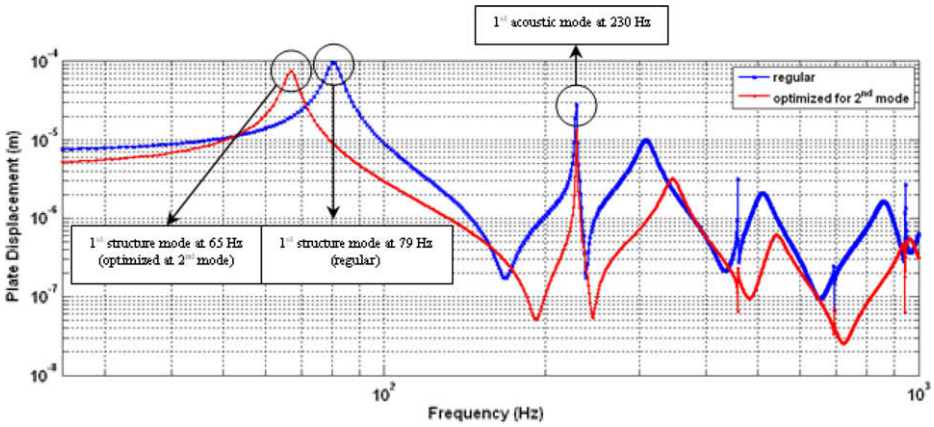

Fig. 11. Displacements of plain plate and topology optimized plate targeting second odd mode.

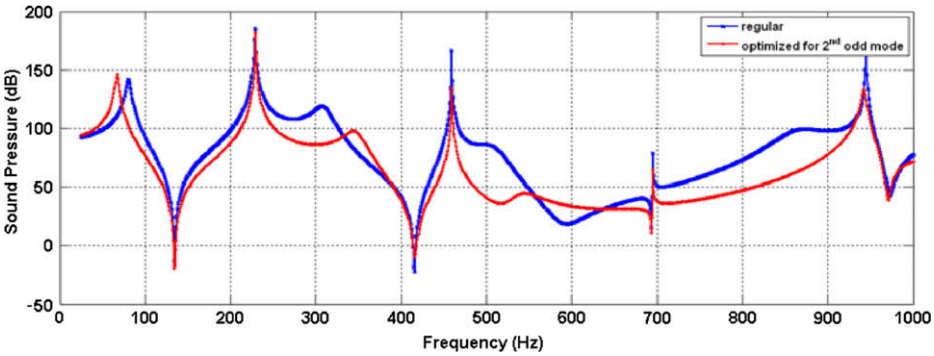

Fig. 12. Sound pressure of plain plate and topology optimized plate targeting second odd mode.

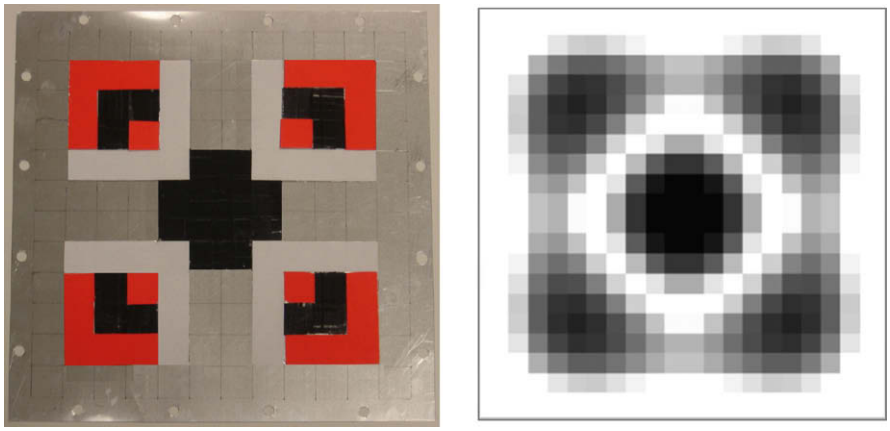

Fig. 13. Manufactured plate approximating the optimization results when targeting the first odd mode.

6. Conclusions

A topology optimization approach was developed for fluid–structure interaction between a flexible plate coupled with a rigid acoustic cavity. The objective of the optimization was to redistribute the material of the flexible plate in order to minimize the fluid–structure coupling. A finite element model was developed to simulate the fluid–structure interactions and was integrated with the topology optimization approach. The model was used to develop the sensitivity analysis necessary

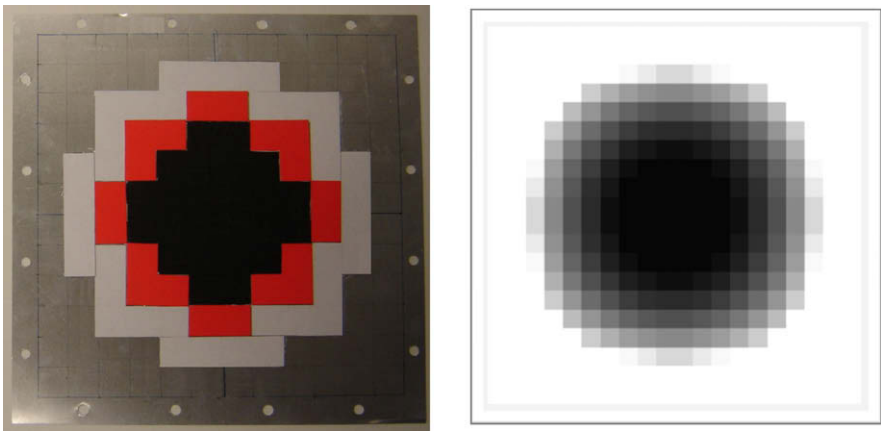

Fig. 14. Manufactured plate approximating the optimization results when targeting the second odd mode.

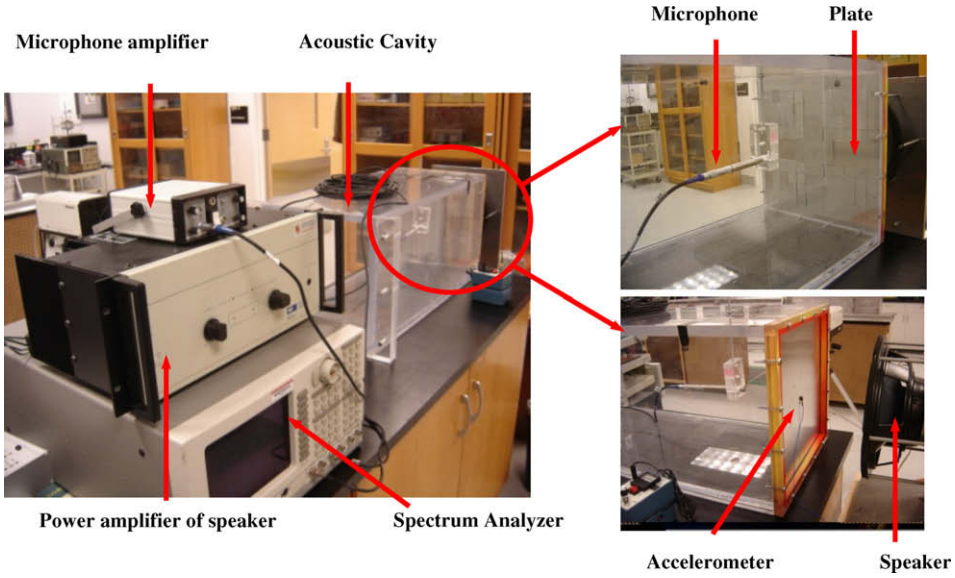

Fig. 15. Experimental setup.

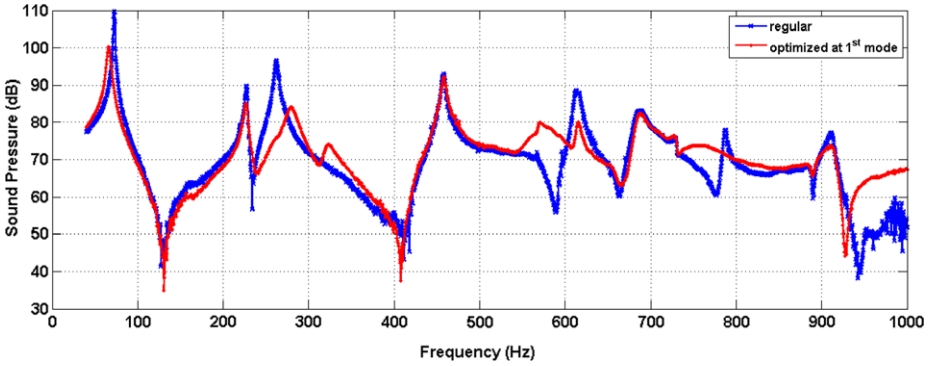

Fig. 16. Experimental sound pressure of plain plate and topology optimized plate targeting first odd mode.

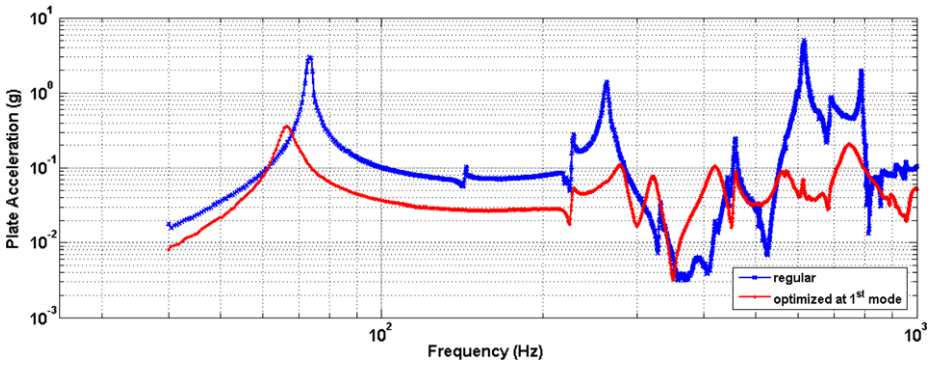

Fig. 17. Experimental accelerations of plain plate and topology optimized plate targeting first odd mode.

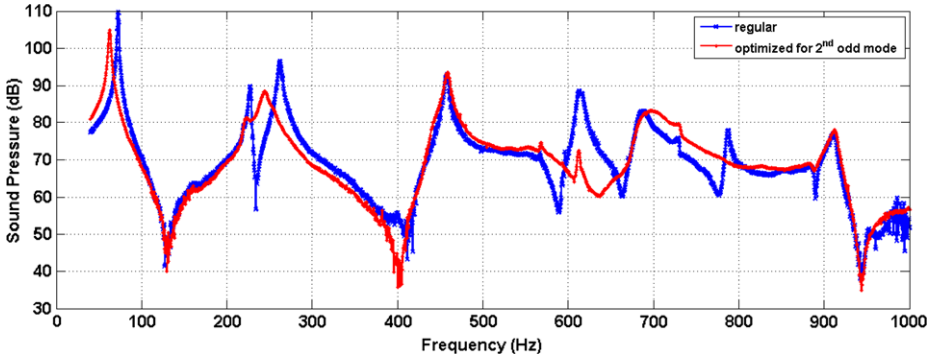

Fig. 18. Experimental sound pressure of plain plate and topology optimized plate targeting second odd mode.

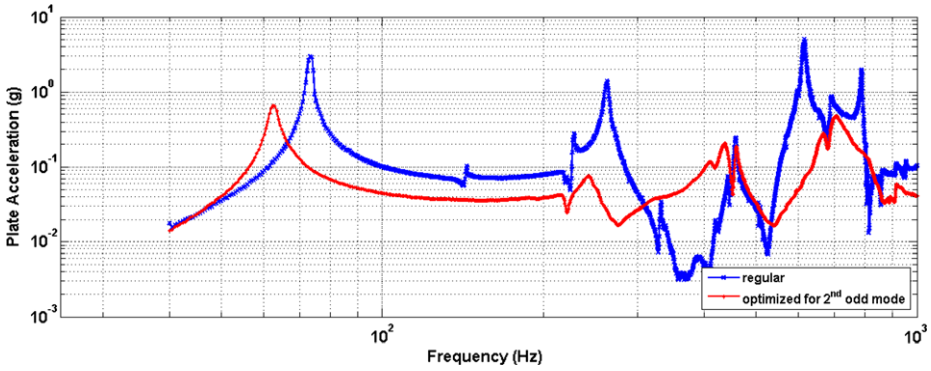

Fig. 19. Experimental accelerations of plain plate and topology optimized plate targeting second odd mode.

for the operation of the topology optimization algorithm. The excitation acting on the plate was locked at the first or second structural odd modes to ensure the effectiveness of the optimization in reducing the sound pressure at the modal frequencies. The analytical model showed considerable attenuation for the first structural odd mode as well as consecutive modes, when the optimization was targeting that mode specifically. On the other hand excellent attenuation was obtained for the second structural odd mode, when targeting the optimization scheme towards that specific mode.

Experimental verification was carried out by manufacturing a set of topology optimized plates that approximate the results obtained from the analytical model. The plates were coupled to an acoustic cavity. Plate vibration acceleration and sound pressure inside the acoustic cavity were measured and compared with the plain-plate case. Considerable attenuation in both the plate vibration acceleration and sound pressure inside the acoustic cavity were recorded. A good match with the

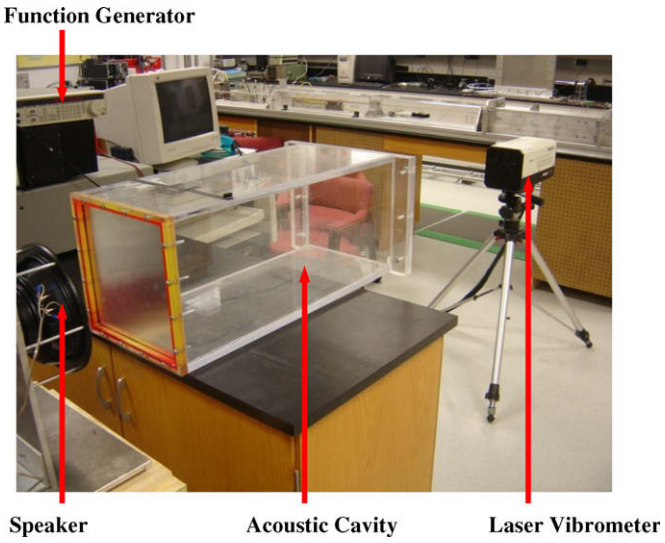

Fig. 20. Laser vibrometer experimental setup.

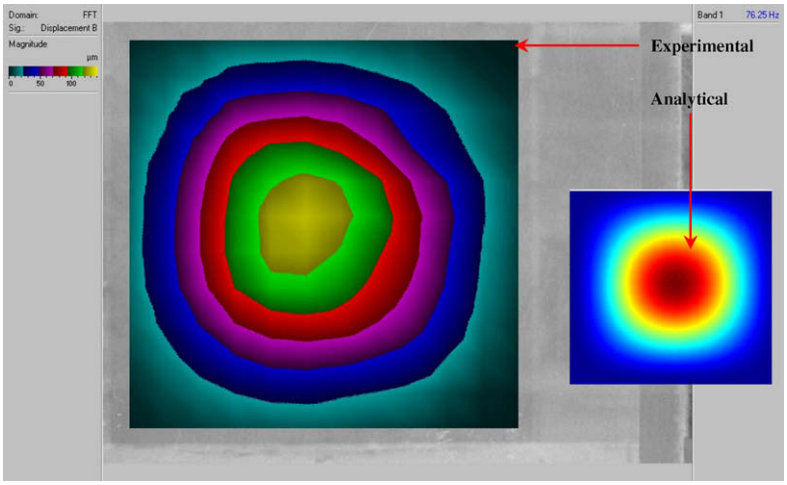

Fig. 21. Displacement field for the plain plate excited at the first structural odd mode.

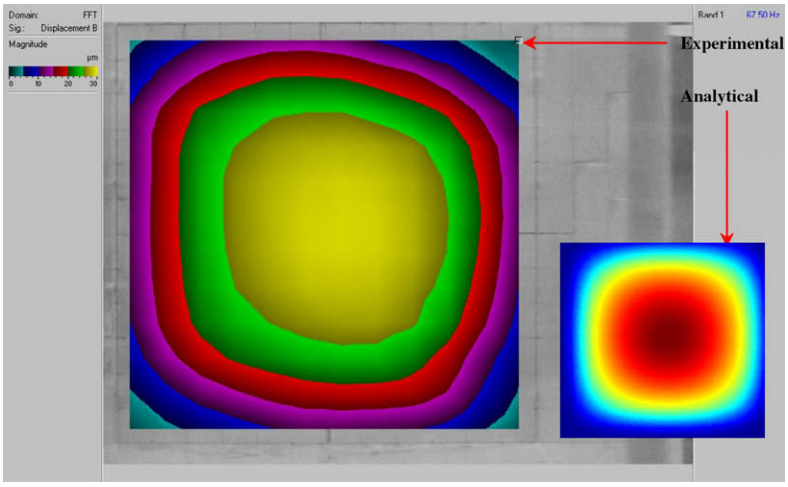

Fig. 22. Displacement field for the plate optimized for the first structural odd mode.

analytical model was observed. The displacement fields of the plate were also measured using a laser vibrometer, and good agreement was observed with the analytical case.

The presented topology optimization approach can be an invaluable tool in the design of a wide variety of critical structures which must operate quietly when subjected to fluid loading. Note that the utility of such a design tool is enhanced through the use of the first order shear deformation theory which makes the analysis equally applicable to thin and thick plate structures. Therefore, a natural extension of the present work is to theoretically predict and experimentally validate the performance of topology optimized thick plates coupled with acoustic cavities.

Acknowledgement

This work has been funded by a grant from the Office of Naval Research (N000140010273). Special thanks are due to Dr. Kam Ng, the technical monitor, for his invaluable inputs and comments.

References

Bendsoe, M.P., 1989. Optimial shape design as a material distribution problem. Structural Optimization 1, 193–202.
Bendsoe, M.P., Diaz, A.R., 1994. Optimization of material properties for improved frequency response. Structural Optimization 7, 138–140.
Bendsoe, M.P., Kikuchi, N., 1988. Generating optimal topologies in structural design using a homogenization method. Computer Methods in Applied Mechanics and Engineering 71 (2), 197–224.
Bendsoe, M.P., Sigmund, O., 2003. Topology Optimization, Theory, Methods and Applications. Springer, Berlin.
Bruyneel, M., Duysinx, P., Fleury, C., 2002. A family of MMA approximations for structural optimization. Structural Multidisciplinary Optimization, 263–276.
Du, Jianbin, Olhoff, Niels, 2007. Minimization of sound radiation from vibrating bi-material structures using topology optimization. Structural Multidisciplinary Optimization, 305–321.
Jensen, J.S., Pedersen, N.L., 2006. On maximal eigenfrequency separation in two-material structures: the 1D and 2D scalar cases. Journal of Sound and Vibration 289, 967–986.
Jog, C.S., 2002. Topology design of structures subjected to periodic loading. Journal of Sound and Vibration 253 (3), 687–709.
Krog, L.A., Olhoff, N., 1999. Optimum topology and reinforcement design of disk and plate structures with multiple stiffness and eigenfrequency objectives. Computers and Structures 72, 535–563.
Olhoff, N., Du, J. 2005. Topology optimization of structures against vibration and noise. In: Proceedings of the 12th International Congress on Sound and Vibration, ICSV12. Lisbon, Portugal, 20 pp.
Pederson, N.L., 2000. Maximization of eigenfrequencies using topology optimization. Structural and Multidisciplinary Optimization 20, 2–11.
Svanberg, K. 1999. The MMA for modeling and solving optimization problems. In: Proceedings of the Third World Congress of Structural and Multidisciplinary Optimization, New York.
Yoon, G.H., Jensen, J.S., Ole, S., 2007. Topology optimization of acoustic–structure interaction problems using a mixed finite element formulation. International Journal for Mechanical Methods in Engineering 70, 1049–1075.